Line-by-line far-infrared spectra of HCl in dense Ar: Asymmetric profiles

A. Medina, S. Velasco, and A. Calvo Hernández
Departamento de Física Aplicada, Universidad de Salamanca, 37008-Salamanca, Spain
(Received 29 July 1991; revised manuscript received 19 November 1991)

A previously reported spectral theory [Phys. Rev. A **44**, 3023 (1991)] is used to analyze the existence of a highly density-dependent asymmetry in the rotational lines of the far-infrared spectrum of HCl in Ar at 162.5 K and densities between 100 and 480 amagat. This asymmetry is explained in terms of dispersive components due to considering mixing effects between lines. In particular, the rotational lines making up the spectrum have a super-Lorentzian (sub-Lorentzian) shape in the low- (high-) frequency side.

PACS number(s): 33.10.Cs, 33.10.Ev, 33.20.Ea, 33.70.Jg

In a recent work [1] (hereafter referred to as I) the influence both of the memory and mixing (nonadditivity) effects in the far-infrared spectra of HCl in Ar at moderate densities (between 100 and 480 amagat) was quantitatively analyzed. From this study, two main conclusions were extracted.

(i) Memory effects, i.e., the existence of a finite correlation time for the absorber-perturber interaction, are not important at all considered densities.

(ii) Mixing effects between lines are very significant at all reported densities, especially far from the centers of the absorption lines where the observed profiles are markedly non-Lorentzian, in agreement with previous theoretical and experimental studies on the vibration-rotation band shapes both for diatom-atom [2–5] and for molecule-molecule [6–10] systems.

In paper I, the analysis of memory and mixing effects was made on the basis of considering the spectra as a whole. This Brief Report is devoted to presenting a line-by-line study. In particular, explicit calculations of the dispersive components associated with mixing effects show the existence of a significant asymmetry in the rotational lines, yielding super-Lorentzian (sub-Lorentzian) lines in the low- (high-) frequency side.

The theoretical model has been described in detail in I. From Eqs. (3.4)–(3.6) in that paper, it is straightforward to obtain that, under Markovian conditions, the theoretical dipolar absorption coefficient $\alpha^M(\omega)$ can be written as a superposition of contributions from individual rotational lines in the form

$$\alpha^M(\omega)=\sum_j \alpha_j^M(\omega)=\sum_j [\alpha_{0j}^M(\omega)+\alpha_{1j}^M(\omega)] , \tag{1}$$

with

$$\alpha_{0j}^M(\omega)=f(\omega)(j+1)e^{-\beta Bhcj(j+1)}\mathrm{Re}[\Lambda_{j+1,j}^M(\omega)] , \tag{2}$$

$$\begin{aligned}\alpha_{1j}^M(\omega)=&\tfrac{1}{3}\hbar^{-2}\lambda^2 f(\omega)(j+1)e^{-\beta Bhcj(j+1)}([(j+2)/(2j+3)]\mathrm{Re}\{\Lambda_{j+2,j+1}^M(\omega)\Lambda_{j+1,j}^M(\omega)[C(\omega_{j+1,j+2})+C(\omega_{j+1,j})]\}\\&+[j/(2j+1)]\mathrm{Re}\{\Lambda_{j,j-1}^M(\omega)\Lambda_{j+1,j}^M(\omega)[C(\omega_{j-1,j})+C(\omega_{j+1,j})]\}\\&+\{2/[(2j+1)(2j+3)]\}\mathrm{Re}[\Lambda_{j,j+1}^M(\omega)\Lambda_{j+1,j}^M(\omega)C(\omega_{j+1,j})]) ,\end{aligned} \tag{3}$$

where

$$f(\omega)=(4\pi n\omega/3\hbar c)(1-e^{-\beta h\omega})\mu^2 , \tag{4}$$

$$\Lambda_{j'j}^M(\omega)=i[\omega-(\omega_{j'j}+\Delta_{j'j})+i\Gamma_{j'j}]^{-1} , \tag{5}$$

$$\Delta_{j'j}=\mathrm{Im}(R_{j'j}) , \tag{6}$$

$$\Gamma_{j'j}=\mathrm{Re}(R_{j'j}) , \tag{7}$$

$$\begin{aligned}R_{j'j}=&\tfrac{1}{3}\hbar^{-2}\lambda^2\{[1/(2j+1)][(j+1)C(\omega_{j+1,j})\\&+jC(\omega_{j-1,j})]\\&+[1/(2j'+1)][(j'+1)C(\omega_{j'j'+1})\\&+j'C(\omega_{j'j'-1})]\} ,\end{aligned} \tag{8}$$

$$C(\omega)=(-i\omega+t_c^{-1})^{-1} . \tag{9}$$

In the above equations n is the number density of the polar active molecules, μ is the permanent dipole moment of the diatomic, $\omega_{j',j}$ means the Bohr frequencies of a quantum rigid rotor, and λ^2 and t_c are two phenomenological parameters denoting, respectively, the squared absorber-perturber interaction strength and its correlation time.

Equation (1) shows that each absorption line $\alpha_j^M(\omega)$ is the sum of two terms: a Lorentzian (secular contribution) line $\alpha_{0j}^M(\omega)$ with half width $\Gamma_{j+1,j}$ and shift $\Delta_{j+1,j}$, Eqs. (2) and (5); and a dispersive (interference contribution) component $\alpha_{1j}^M(\omega)$, Eq. (3), which accounts for the

mixing effects between the absorption line $j \rightarrow j+1$ with the $j+1 \rightarrow j+2$ line (first resonant term R1), with the $j-1 \rightarrow j$ line (second resonant term R2) and with the emission $j+1 \rightarrow j$ line (antiresonant term AR).

Now, the theory is applied to analyze the asymmetry induced by the dispersive components in the different rotational lines making up the theoretical spectrum for HCl dissolved in dense Ar at $T=162.5$ K and at Ar densities of 100, 200, 300, 400, and 480 amagat. The values of the stochastic parameters involved in the theory, λ^2 and t_c, are summarized in Table I in I.

Figures 1–3 show the behavior of some j-rotational transition lines for the HCl-Ar system at 100, 300, and 480 amagat (at the remaining Ar densities of 200 and 400 amagat an intermediate behavior is observed). In these figures the upper, intermediate, and lower drawings show, respectively, the shape of some secular, interference, and final lines. In these figures, as well as in the following, the normalization has been chosen so that the maximum value of $\alpha^M(\omega)$ $[=\sum_j \alpha_j^M(\omega)]$, with $0 \le j \le 10$, will be unity for each density. Dotted lines in Figs. 1(c)–3(c) show $\alpha^M(\omega)$.

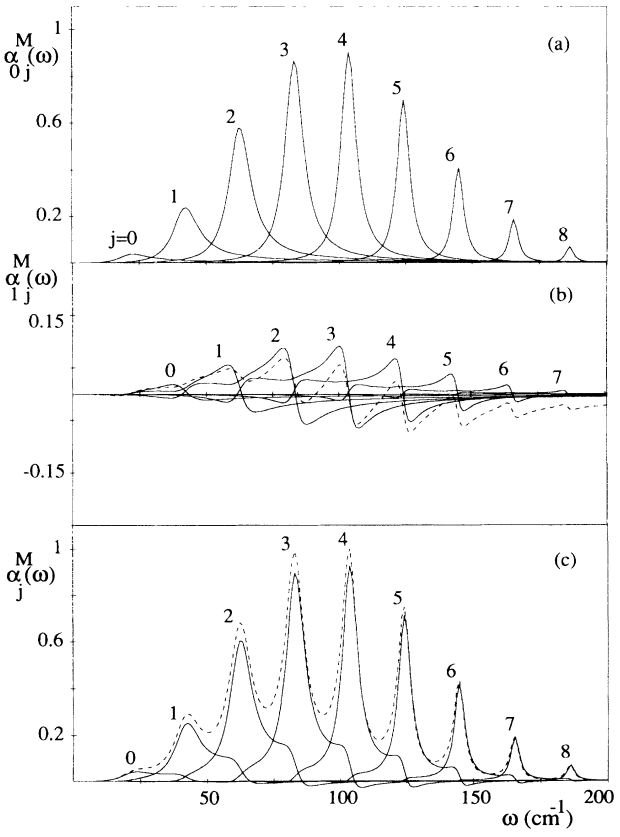

FIG. 1. Markovian line-by-line profiles for the HCI-Ar system at 100 amagat and 162.5 K, obtained with values for the parameters λ and t_c collected in Table I in I. Each line is indicated by the initial j of the rotational transition. (a) Secular profiles $\alpha_{0j}^M(\omega)$, Eq. (2); (b) interference components $\alpha_{1j}^M(\omega)$, Eq. (3); (c) total profiles $\alpha_j^M(\omega)=\alpha_{0j}^M(\omega)+\alpha_{1j}^M(\omega)$. Dashed line in (b) is $\alpha_1^M(\omega)=\sum_j \alpha_{1j}^M(\omega)$ and dashed line in (c) is $\alpha^M(\omega)=\sum_j \alpha_j^M(\omega)$ $0 \le j \le 10$.

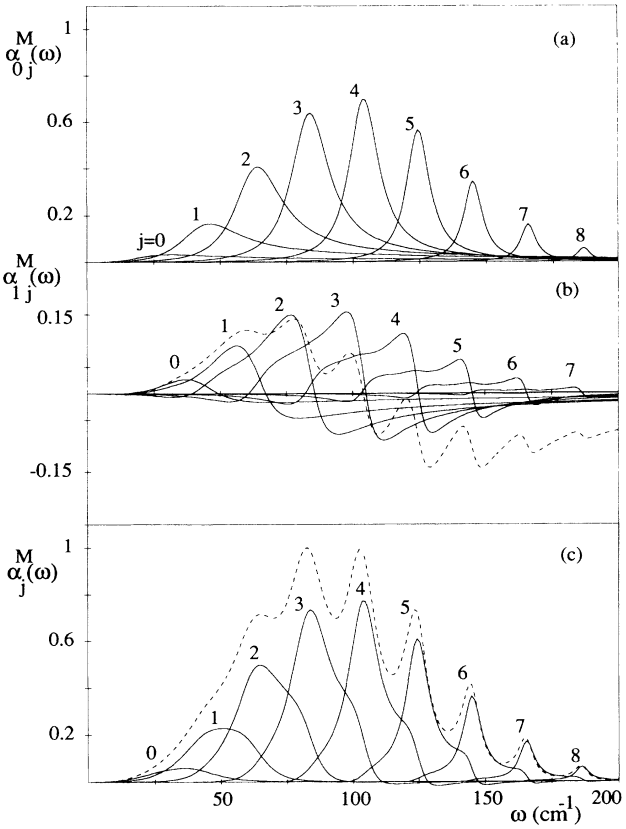

FIG. 2. Same as Fig. 1, but at 300 amagat.

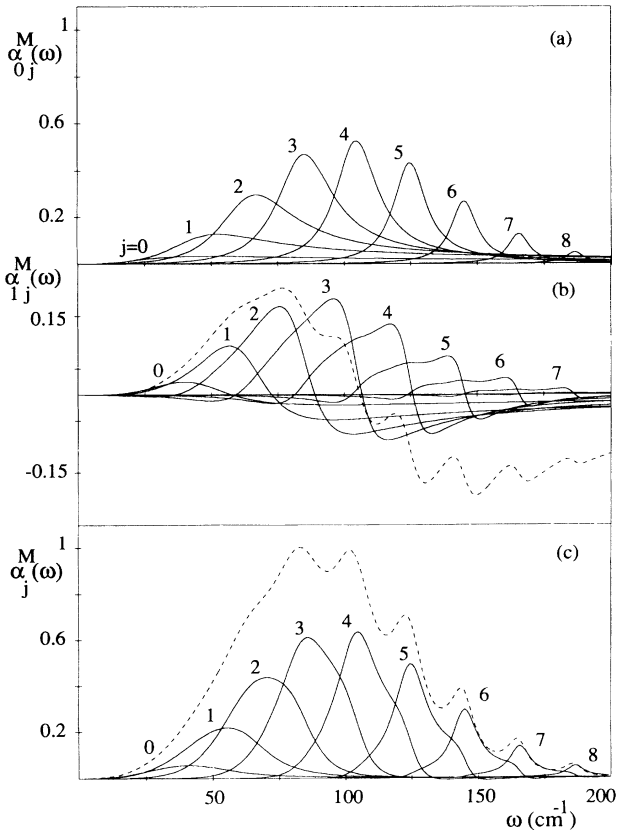

FIG. 3. Same as Fig. 1, but at 480 amagat.

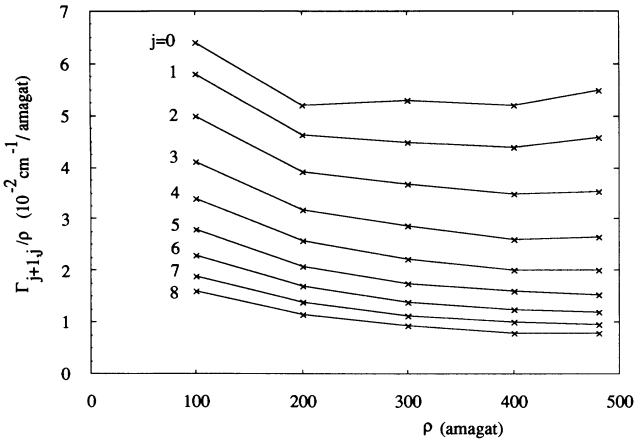

FIG. 4. The ratio between the theoretical secular half width (see text) of several rotational lines and the Ar density as a function of the density at $T=162.5$ K. Each line is indicated by the initial j of the rotational transition.

From Fig. 1(a), it is clear for low densities that each rotational transition line in the secular approximation $\alpha_{0j}^{M}(\omega)$ is a well-distinguishable and relatively well-isolated line, located very close to the Bohr frequency $\omega_{j+1,j}$. When we go from low to high densities [Figs. 2(a) and 3(a)] each secular line becomes broader and it is placed far from $\omega_{j+1,j}$, especially for low j transitions which become indistinguishable. The variation with the Ar density of the theoretical secular half widths $\Gamma_{j+1,j}$ [see Eq. (7)] for several rotational lines is plotted in Fig. 4. In this figure, a nonlinear behavior is observed which is in qualitative agreement with other theoretical calculations [11,12] and with the corresponding experimental $\Gamma_{j+1,j}^{\text{expt}}$ set [13] (see Fig. 3 in Ref. [13] and Fig. 8 in Ref. [11]). However, significant numerical differences between $\Gamma_{j+1,j}$ and $\Gamma_{j+1,j}^{\text{expt}}$ are observed. This is because of the theoretical $\Gamma_{j+1,j}$ set corresponds to the half widths of the secular rotational lines in our spectral theory (i.e., without taking into account the interference contribution), while the experimental $\Gamma_{j+1,j}^{\text{expt}}$ set was obtained from a fitting procedure between the experimental profile and a sum of individual lines of van Vleck–Weisskopf type [11,13]. In fact, the observed numerical differences between $\Gamma_{j+1,j}$ and $\Gamma_{j+1,j}^{\text{expt}}$ are indicative of the importance of mixing effects between adjacent rotational lines in our theory.

As can be checked in Figs. 1(b)–3(b), the dispersive lines $\alpha_{1j}^{M}(\omega)$ produce, essentially, a positive absorption at frequencies placed on the left-hand side of the centers of the secular lines $\alpha_{0j+1}^{M}(\omega)$ and a negative and less intense absorption at frequencies placed on the right-hand side. This pattern is due to the behavior of the resonant R1 and R2 terms, which is plotted in Fig. 5 for two representative j-transition lines ($j=3,6$) at the two extreme densities of 100 and 480 amagat. The antiresonant AR term is negligible in comparison with the resonant R1 and R2 terms and, then, it is not considered in Fig. 5 (at all densities and j values considered here, the values of the AR term were found to be less than the values of R1 and R2 by at least a factor of 100).

The rotational lines $\alpha_{j}^{M}(\omega)=\alpha_{0j}^{M}(\omega)+\alpha_{1j}^{M}(\omega)$ are plotted in Figs. 1(c)–3(c). At all considered densities, each $\alpha_{j}^{M}(\omega)$ presents noticeable differences with respect to the secular lines $\alpha_{0j}^{M}(\omega)$ due to the dispersive component $\alpha_{1j}^{M}(\omega)$. These differences can be summarized as follows.

(i) At low density [Fig. 1(c)] and low j values ($j<6$), the main difference is made of a double shoulder at the wings of $\alpha_{j}^{M}(\omega)$. The right-sided one, which is more pronounced, is located in the trough of the secular lines $\alpha_{0j}^{M}(\omega)$ and $\alpha_{0j+1}^{M}(\omega)$; the left-sided one, which is smoother, is located in the trough of the secular lines $\alpha_{0j}^{M}(\omega)$ and $\alpha_{0j-1}^{M}(\omega)$. Notice that these two adjacent troughs with strong asymmetry correspond, respectively, to frequencies for which the dispersive components $\alpha_{1j}^{M}(\omega)$ and $\alpha_{1j-1}^{M}(\omega)$ achieve their positive maximum values. As the perturber density increases [Figs. 2(c) and 3(c)], the shoulders are only apparent at intermediate j values, although

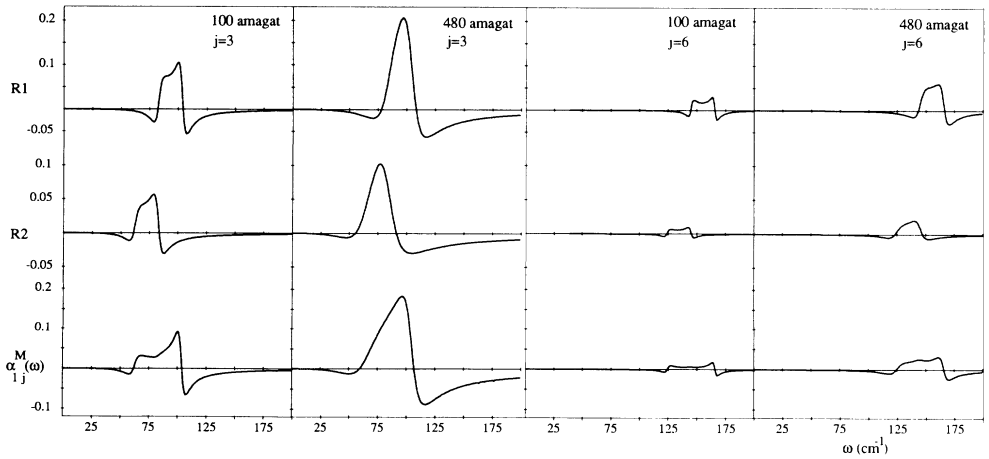

FIG. 5. Density behavior of the R1 and R2 terms (see text) appearing in the dispersive component $\alpha_{1j}^{M}(\omega)$, Eq. (3), for the $j=3,6$ rotational transition lines.

the differences between the secular and resulting rotational lines are greater than those at low densities due to the increasing importance of the mixing effects [1].

(ii) Both at low and high densities the shoulders for high j values ($j>6$) gradually disappear because the intensity of the dispersive components for high frequencies ($\omega>150$ cm^{-1}) is practically negligible in comparison with the intensity of the secular components at the same frequencies.

A straightforward consequence from the asymmetry induced by the dispersive components is the observed behavior in the theoretical lines $\alpha_j^M(\omega)$: super-Lorentzian (sub-Lorentzian) in the low- (high-) frequency side. This result is better understood from Fig. 6, where we have plotted, for 300 amagat, some Lorentzian and interference profiles. It is observed that each dispersive component $\alpha_{1j}^M(\omega)$ achieves its maximum (positive) value in the windows between the $\alpha_{0j}^M(\omega)$ and $\alpha_{0j+1}^M(\omega)$ secular lines and a maximum (negative) value in the windows between the $\alpha_{0j+1}^M(\omega)$ and $\alpha_{0j+2}^M(\omega)$ secular lines, being negative or near zero otherwise. In the troughs between two low secular lines, for instance, $j=2$ and 3, the positive-dispersive contribution is greater than the negative-dispersive contribution, while in the troughs between two high rotational lines, for instance $j=6$ and 7, it is the negative-dispersive contribution that predominates over the positive part. So, positive-dispersion components at low frequencies progressively transform into negative-dispersion components at high frequencies. Thus super-Lorentzian behavior of the low j-rotational lines becomes sub-Lorentzian behavior for the high j-rotational lines.

We note the great similarity between Fig. 6 in this paper and a scheme on the influence of the dispersive components due to line coupling for some j lines in the R branch of the self- and N_2-broadened ν_3 CO_2 vibration-rotation band (cf. Fig. 9 in Ref. [7]).

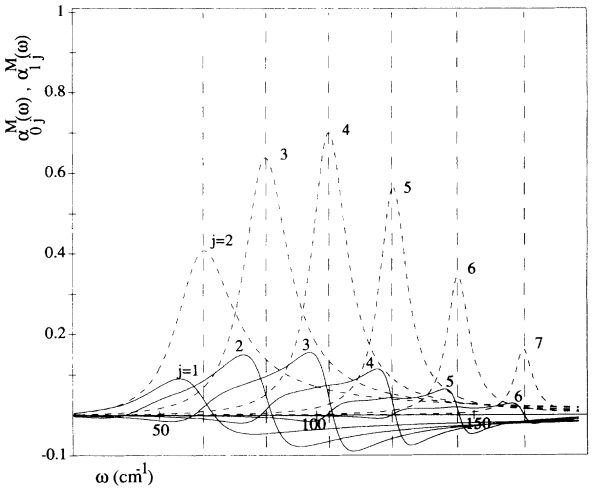

FIG. 6. Influence of the interference components $\alpha_{1j}^M(\omega)$ (——) on the secular profiles $\alpha_{0j}^M(\omega)$ (· · · ·) due to line mixing for some j-rotational transition lines at 300 amagat. Vertical dash-dotted lines denote the positions of the maxima for $\alpha_{0j}^M(\omega)$.

This work was partially supported by the DGICYT of España (Grant No. PS89-0160) and by a Grant from Programa de Acciones Concertadas of the Universidad de Salamanca.

[1] A. Medina, S. Velasco, and A. Calvo Hernández, Phys. Rev. A **44**, 3023 (1991).
[2] Ph. Marteau, C. Boulet, and D. Robert, J. Chem. Phys. **80**, 3632 (1984).
[3] J. Boissoles, C. Boulet, D. Robert, and S. Green, J. Chem. Phys. **87**, 3436 (1987).
[4] S. Green, J. Boissoles, and C. Boulet, J. Quant. Spectrosc. Radiat. Transfer **39**, 33 (1988).
[5] J. Boissoles, C. Boulet, D. Robert, and S. Green, J. Chem. Phys. **90**, 5392 (1989).
[6] M. D. Bulanin, A. B. Dokuchaev, M. V. Tonkov, and N. N. Filippov, J. Quant. Spectrosc. Radiat. Transfer **31**, 521 (1984).
[7] C. Cousin, R. LeDoucen, C. Boulet, A. Henry, and D. Robert, J. Quant. Spectrosc. Radiat. Transfer **36**, 521 (1986).
[8] J. Boissoles, C. Boulet, L. Bonamy, and D. Robert, J. Quant. Spectrosc. Radiat. Transfer **42**, 509 (1989).
[9] S. Green, J. Chem. Phys. **90**, 3603 (1989).
[10] C. Boulet, J. Boissoles, and D. Robert, J. Chem. Phys. **89**, 625 (1988).
[11] C. Boulet, D. Robert, and L. Galatry, J. Chem. Phys. **72**, 751 (1980).
[12] S. Green, J. Chem. Phys. **92**, 4679 (1990).
[13] D. Frenkel, D. J. Gravesteyn, and J. v. der Elsken, Chem. Phys. Lett. **40**, 9 (1976).